An Active Damper to Suppress Multiple Resonances with Unknown Frequencies

Xiongfei Wang, Frede Blaabjerg, and Marco Liserre
Department of Energy Technology, Aalborg University, Aalborg, Denmark
xwa@et.aau.dk, fbl@et.aau.dk, mli@et.aau.dk

***Abstract*—The increasing use of power electronics devices tends to aggravate high-frequency harmonics and trigger resonances across a wide frequency range into power systems. This paper presents an active damper to suppress multiple resonances with unknown frequencies. The active damper is realized by a high-bandwidth power converter that can selectively dampen out the wideband resonances. A cascaded adaptive notch filter structure is proposed to detect the frequencies of resonances, which makes the active damper different from the resistive-active power filter for harmonic resonance suppression. The performance of the active damper is validated by implementing it to suppress the resonances in a grid-connected inverter with a long power cable. The results show that the active damper can become a promising approach to stabilizing the future power electronics based power systems.**

I. INTRODUCTION

There is a growing demand on the use of power electronics converters to connect renewable energy sources and industrial drives to the electrical grids [1]. Power electronics is enabling the development of the energy-efficient, sustainable and smart power systems [2]. With the increasing use of high-frequency switching power converters, the power system characteristics have gradually been changed. The high-frequency harmonics tend to be more apparent and the system damping is reduced due to the small time constants of converters. These wideband frequency harmonics may interfere with other devices in the power system and trigger resonances across a wide frequency range [3]. To reduce the high-frequency switching ripples, the high-order power filters are widely adopted for converters [4]. However, the shunt capacitors in these filters may also lead to resonance, which may become more severe when the multiple converters are interconnected [5]-[7]. Further, the widespread use of power cables in the renewable power plants may further aggravate the resonances due to the parasitic capacitances [8].

To address the wideband harmonics and resonances in the future power electronics based power systems, the extensive research works have been made, which either introduce the additional control loop for power converters [9]-[11], or add the passive damping circuit into the filters [12]-[14]. However, most of them are either limited by the dynamic behavior of converters or sensitive to the uncertainties of power system conditions. To overcome these drawbacks, an active damper concept that is based on a high-bandwidth power converter is recently introduced [15]. As opposed to reshaping the terminal behavior of converters, the active damper aims to dynamically suppress the resonances at the Point of Common Coupling (PCC). The active damper can operate in a similar way to the Resistive-Active Power Filter (R-APF) by synthesizing the virtual damping resistances at the resonance frequencies [16]. But instead of damping the low-order harmonic resonances as the R-APF, the active damper only works for the resonances, thus allowing a low power design and high control bandwidth, and thus the detection of resonances becomes more important for the active damper. In [15], the detection and prevention of single resonance is attained, whereas the wideband harmonics in real cases may trigger double or multiple resonances [17].

This paper presents an active damper that can suppress the multiple resonances with unknown frequencies. A cascaded Adaptive Notch Filter (ANF) structure based on the multiple ANFs and Frequency-Locked Loops (FLLs) is proposed to detect the resonance frequencies. Thus, the active damper is enabled to selectively control the resonant voltages by means of multiple frequency adaptive resonant voltage controllers. The performance of the active damper is validated by applying it for a three-phase grid-connected inverter through the long power cable. The results show that active damper provides an effective way to suppress the resonance propagation along the power cable and the output *LCL*-filter of inverter.

II. ACTIVE DAMPER

A. System Configuration

Fig. 1 illustrates a simplified one-line diagram of an active damper for a three-phase voltage source inverter connected to the grid via a long power cable. The grid-side inductor current (i_g) of the *LCL*-filter is controlled for the inverter, such that no additional damping is needed when the *LCL*-filter resonance frequency is higher than the one-sixth of the control sampling frequency [18]. However, the variation of the grid impedance and the parasitic capacitances in the power cable may shift the

This work was supported by European Research Council (ERC) under the European Union's Seventh Framework Program (FP/2007-2013)/ERC Grant Agreement [321149-Harmony].

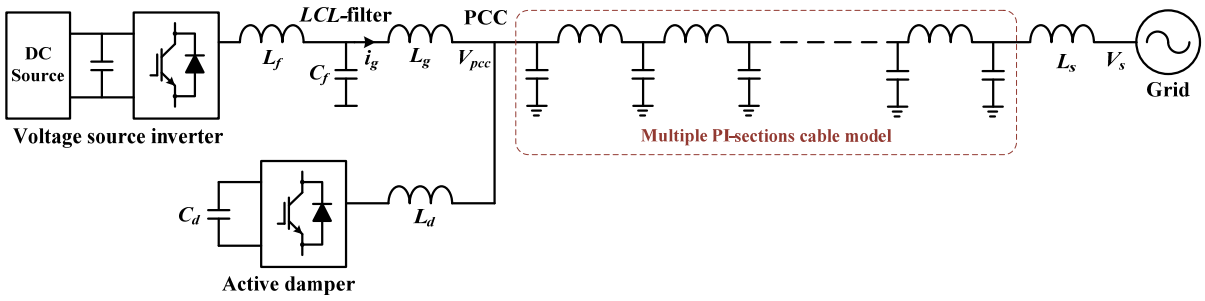

Fig. 1. Simplified one-line diagram of an active damper for a grid-connected voltage source inverter through a long power cable.

actual *LCL*-filter resonance to a lower value, and even trigger the resonances in a wideband [17]. Hence, the active damper is installed at the PCC of inverter to suppress the resonances brought by the different equivalent system impedances.

B. Operation Principle

Fig. 2 illustrates the control diagram for the active damper, where the active damper controls the resonant voltages at the PCC using multiple frequency adaptive resonant controllers in parallel. Fig. 3 (a) depicts the structure of frequency adaptive resonant controller based on two integrators, which is given by

$$G_{rc,i}(s) = \frac{K_{r,i}\omega_{c,i}s}{s^2 + \omega_{c,i}s + \omega_{r,i}^2} \tag{1}$$

where $\omega_{r,i}$ and $\omega_{c,i}$ denote the center frequency and bandwidth of the i-th resonant controller, respectively. $K_{r,i}$ is the gain of the resonant controller. To further improve the accuracy of the resonant controller in the discrete time domain, the sixth-order Taylor series approximation is used to correct the poles of the z-domain transfer function, as shown in Fig. 3 (b) [19].

It is worth noting that the active damper only works at the resonance frequencies, which is different from the APF for the steady-state harmonic compensation. The online detection of resonance frequencies is thus essential for the active damper to selectively control the resonant voltages. Although a number

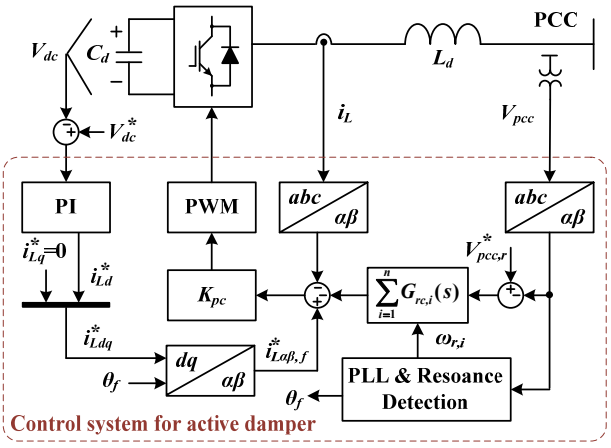

Fig. 2. Control bock diagram of the active damper.

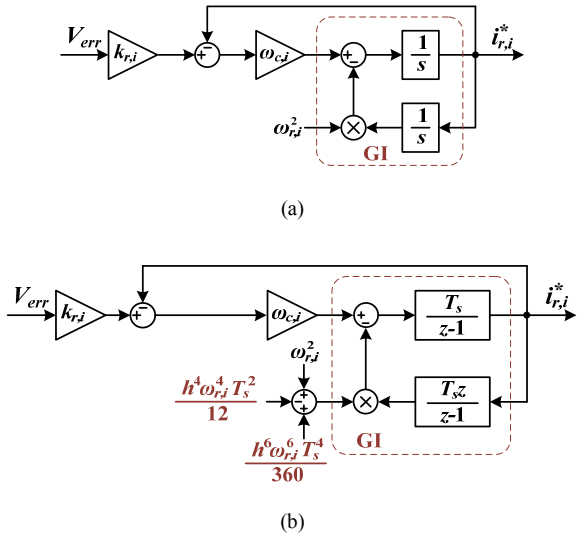

Fig. 3. Block diagram of the resonant controller based on two integrators. (a) Continuous form. (b) Discretized in z-domain.

of harmonic estimation techniques are available [20], [21], the detection of multiple resonances is still a challenge in terms of the computation burden and dynamic performance.

III. Detection of Resonance Frequencies

This section first reviews the main types of the ANF-based Phase-Locked Loop (PLL) or FLL for harmonic detection, and then proposes a cascaded ANF structure for the active damper based on the use of multiple ANFs and FLLs.

A. Overview of ANF-Based PLL/FLL

Fig. 4 depicts the block diagrams of the 1- weight and 2-weight ANFs using the Least Mean Square (LMS) adaptation algorithm [22], [23]. The LMS-based ANFs are introduced for the Active Noise Cancelling (ANC), which are later applied t enhance the phase detection of PLL and generates a series of ANF-based PLL/FLL for the retrieval of sinusoidal signals in noises [24]-[35].

Fig. 5 shows the PLL based on the 1-weight ANF, which is firstly reported as the residual mode PLL in [24], and is then developed as the Magnitude PLL (MPPL) for communication systems [25]-[27], and the Enhanced PLL (EPLL) for power system frequency/phase tracking [28], [29]. Compared to the mixer phase detector, the ANF effectively reduces the second-

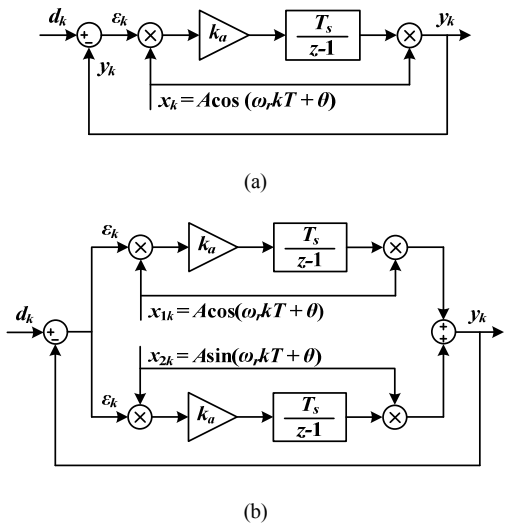

Fig. 4. Block diagrams for (a) 1-weight ANF, and (b) 2-weight ANF based on the LMS adaptation algorithm.

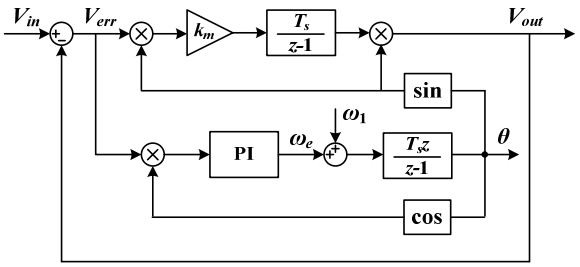

Fig. 5. The 1-weight ANF-based PLL structure.

order harmonic ripple. It has recently been found that several single-phase synchronous reference frame PLLs basically own the same operation principle as the ANF-based PLL [30].

The similar application of the 2-weight ANF for PLL can be found in the Quadrature PLL (QPLL) [31]. Further, due to the equivalence between the continuous forms of the 2-weight ANF and the Generalized Integrator (GI) in Fig. 3, the ANF-based FLLs are developed based on the use of the generalized integrators [32]-[35]. Fig. 6 shows the block diagram of two ANF-based FLLs, where the ANF-based FLL in Fig. 6 (b) is also known as the Second-Order Generalized Integrator FLL (SOGI-FLL) [33]. It is interesting to see that the FLL in Fig. 6 employs the same phase detector as the PLL in Fig. 5, i.e. the product of the input error signal and the quadrature signal.

B. Cascaded ANF Structure

The use of the multiple ANF-based PLL/FLL for harmonic estimation has been reported in [26], [34], where the parallel ANF structure is employed, as depicted in Fig. 7. This method works well for the estimation of harmonic signals which are correlated to the fundamental frequency signal. However, its performance is deteriorated by the presence of interharmonics or resonances [27], [35]. Therefore, to detect the resonances, a cascaded ANF structure is introduced in the following.

Fig. 8 shows the proposed cascaded ANF structure for the

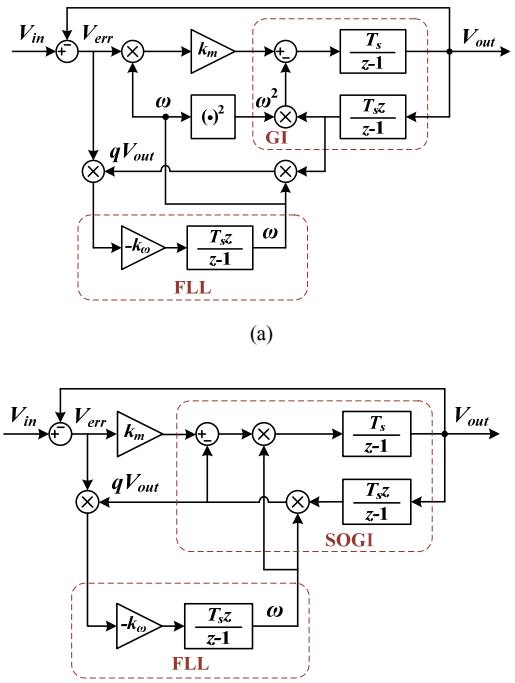

Fig. 6. 2-weight ANF-based FLLs. (a) ANF-based FLL with the generalized integrator. (b) SOGI-FLL.

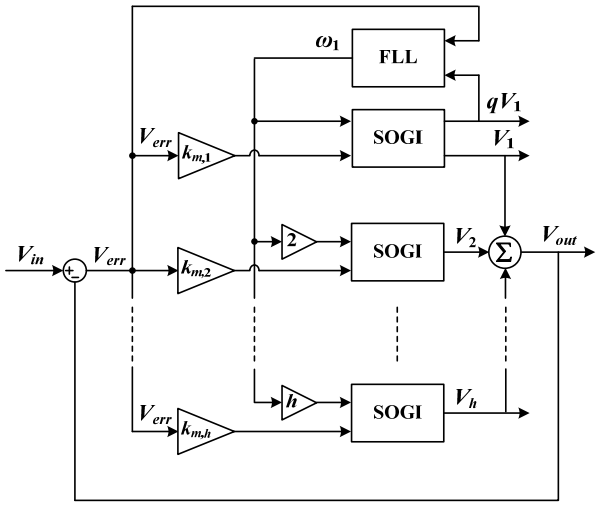

Fig. 7. Parallel ANF structure with a common FLL for harmonic detection.

detection of resonance frequencies. Different from the parallel ANF structure with a common FLL in Fig. 7, multiple ANF-based FLLs are connected in cascade. Further, to decouple the effect of harmonics or interharmonics disturbances next to the resonance frequencies, the Pre-filtered-ANF (P-ANF) method is adopted in each ANF-based FLL, as shown in Fig. 9 [35]. In addition, instead of the SOGI used in Fig. 7, the ANF structure in Fig. 6 (a) is employed for high frequency resonances by means of the GI depicted in Fig. 3(b).

Fig. 10 shows the performance of the proposed cascaded ANF structure for the detection of resonance frequencies. The

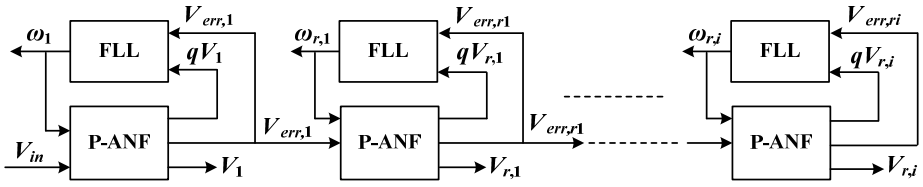

Fig. 8. Proposed cascaded ANF structure with multiple ANF-based FLLs.

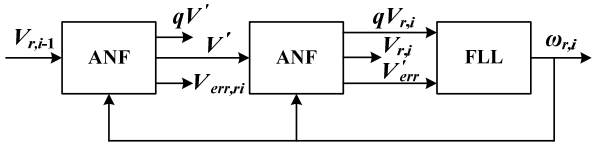

(b)

Fig. 9. Block diagram of the Pre-filtered-ANF (P-ANF).

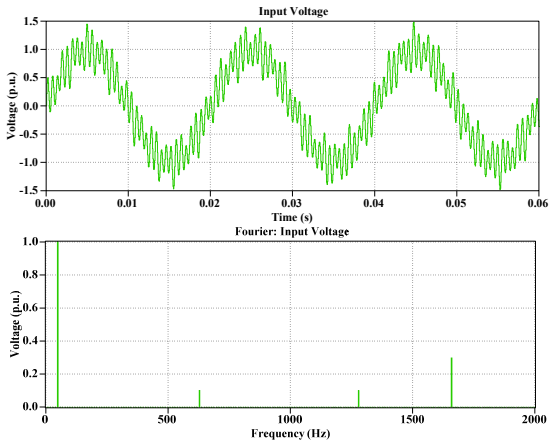

(a)

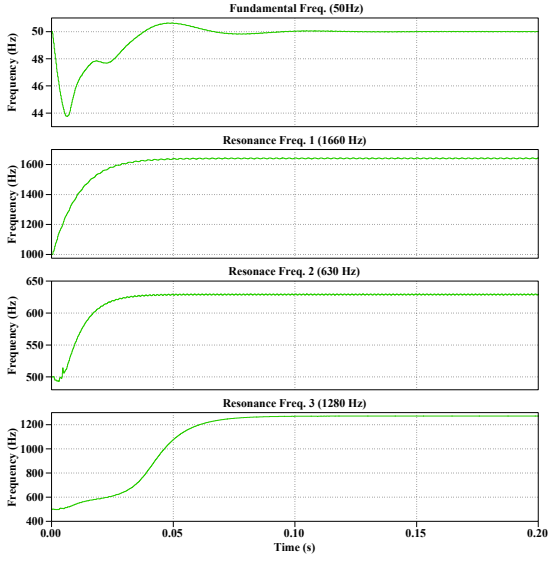

(b)

Fig. 10. Performance of the cascaded ANF structure for detecting multiple resonances. (a) Input voltage waveform and harmonic spectra. (b) Measured fundamental and resonance frequencies.

input voltage signal is disturbed with three resonances at 1660 Hz, 630 Hz, and 1280 Hz, respectively. It is seen that the good resonance frequency detection is attained. Notice that in three-phase systems, due to the presence of the negative-sequence components, the positive-/negative-sequence calculation block needs to be used [34].

IV. Ferquency-Domain Analysis

Fig. 11 depicts the current control loop for grid-connected inverter, where the main parameters are given in Tables I. The Proportional Resonant (PR) current controller in the stationary $\alpha\beta$-frame is adopted for the zero steady state error. Since the resonance frequency of *LCL*-filter is designed higher than the one-sixth of the sampling frequency, no active damping loop is considered. To see the effect of the power cable and the grid impedance, the open-loop gains of the current control loop are derived as follows

$$T_c(s) = \frac{Z_{Cf} G_c G_d}{Z_{Lf} Z_{Cf} + Z_{Lf} Z_{Lg} + Z_{Cf} Z_{Lg}} \tag{2}$$

$$T_{ce}(s) = \frac{Z_{Cf} G_c G_d}{Z_{Lf} Z_{Cf} + Z_{Lf} (Z_{Lg} + Z_{eq}) + Z_{Cf} (Z_{Lg} + Z_{eq})} \tag{3}$$

where $Z_{eq}(s)$ is the equivalent system impedance of inverter derived from the PCC, which includes the grid impedance and the cable impedance. $T_c(s)$ and $T_{ce}(s)$ are the loop gains with and without the equivalent system impedance, respectively.

TABLE I. System Electrical Parameters

Parameters	Symbol	Value
Grid votlage	V_s	400 V/50 Hz
Grid inductance	L_s	5 mH
Cable inductance per section	L_l	0.8 mH
Cable resistance per section	r_l	0.025 Ω
Cable capacitance per section	C_l	4.7 μF
LCL-filter inductor (grid-side)	L_g	0.9 mH
LCL-filter capacitor	C_f	10 μF
LCL-filter inductor (inverter-side)	L_f	3 mH
Inverter switching frequency	f_{sw}	10 kHz
Filter inductor of active damper	L_d	3 mH
Active damper switching frequency	f_{swd}	20 kHz

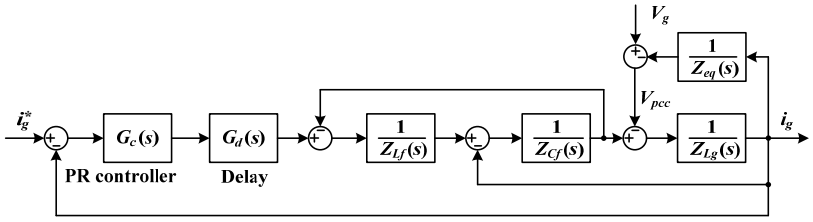

Fig. 11. Block diagram for the current control loop of grid-connected inverter.

$G_c(s)$ is the PR current controller and $G_d(s)$ denotes the effect of the computation and pulse width modulation delay involved in the digital control system.

Fig. 12 compares the root loci for the current control loop with and without the equivalent system impedance at the PCC. It is seen that two resonant pole pairs are moved outside the unit circle by the presence of power cable and grid impedance. This fact implies that two unstable resonance peaks will arise even for the stable current controller designed on the basis of the *LCL*-filter plant.

To further identify the frequencies of resonances, Fig. 13 compares the frequency responses of the current control loop gains with and without the equivalent system impedance. It is noted that a stable current controller is designed for the current control loop without the equivalent system impedance at the PCC. In contrast, the parasitic capacitances of the power cable bring in multiple resonance peaks. However, it is worth noting that not all of these resonance peaks will result in the unstable current control loop. By taking a closer look at the phase-frequency response, it can be found from the Nyquist stability criterion that two unstable resonance peaks occur around the frequencies of 1000 Hz and 1550 Hz, respectively, with the same current controller. Hence, the active damper is needed to suppress these resonances.

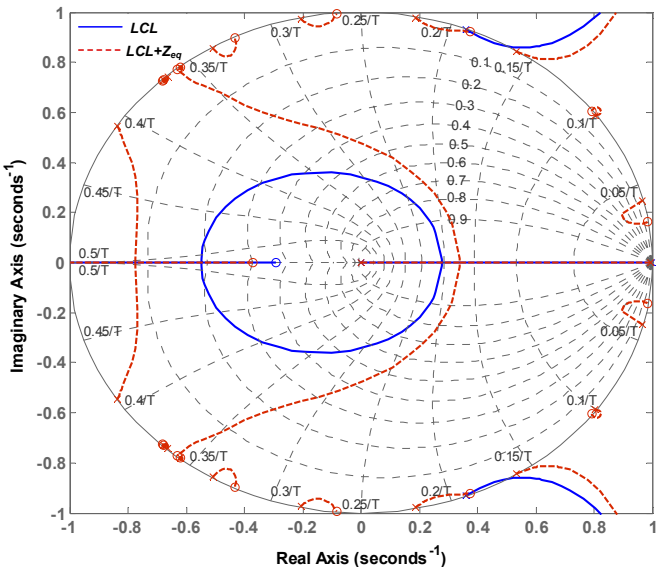

Fig. 12. Root loci of the current control loop with and without the equivalent system impedance at the PCC.

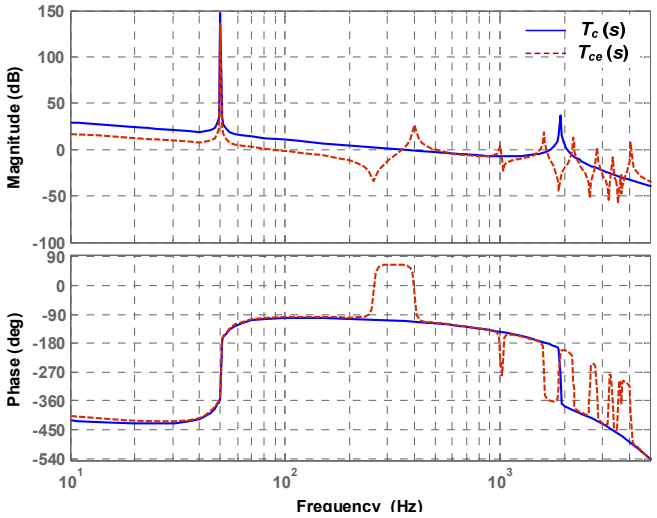

Fig. 13. Comparison of frequency responses of the open-loop gain of current control loop with and without the equivalent system impedance at the PCC.

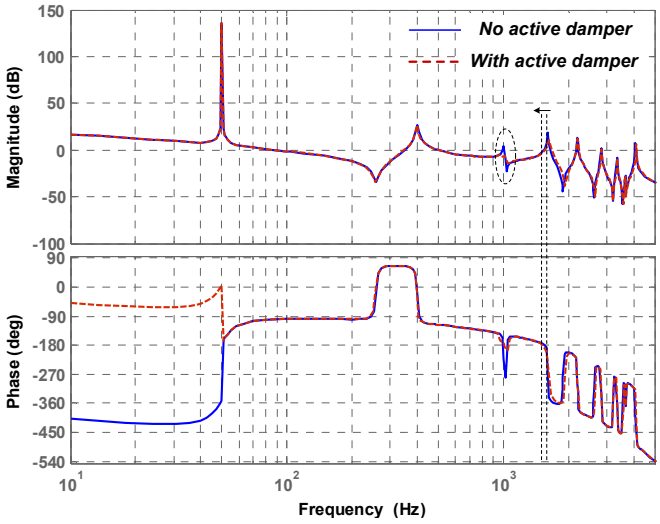

Fig. 14. Stabilizing effect of the active damper in the frequency-domain.

Fig. 14 shows the stabilizing effect of the active damper in the frequency-domain. The active damper can be represented by the resonant voltage controllers expressed in (1) in the frequency-domain, where the gains of resonant controllers are equal to the reciprocal of equivalent resistances synthesized by the active damper [15]. It is interesting to note that the active damper has the different stabilizing effect for the two unstable

resonance peaks. The resonance peak near 1000 Hz is reduced below 0 dB, whereas the phase crossing over 180 degree at the resonance around 1550 Hz is shifted to the frequency with the magnitude below 0 dB. Consequently, the unstable resonances are effectively suppressed by the active damper. The design of the resonant voltage controllers can also be derived from this frequency-domain analysis.

V. Simulation Results

To further confirm the performance of the active damper, the nonlinear time domain simulations for the system shown in Fig. 1 are carried out in MATLAB/SIMULINK and PLECS Blockset. The parameters listed in Table I are adopted for the simulation model.

First, to see the effect of the system equivalent impedance on the stability of the current control loop, Fig. 15 shows the simulated PCC voltage and grid current of the grid-connected inverter without enabling the active damper. The inverter is switched from the ideal AC voltage source to the power cable at the time instant of 0.2 s. It is obvious that the current control loop becomes unstable due to the effect of system equivalent impedance, which confirms the root locus analysis in Fig. 12. The corresponding harmonic spectra for the PCC voltage and the grid current of the inverter are depicted in Fig. 16. Since the unstable resonances are gradually magnified, the harmonic spectra are obtained by sampling one fundamental period. It is seen that two resonance peaks are triggered around 1000 Hz and 1550 Hz, respectively, in the grid current, which validates the frequency response shown in Fig. 13.

Then, to see the selective resonance damping performance, the active damper is firstly enabled to suppress the resonance around 1000 Hz. Fig. 17 depicts the simulated PCC voltage and grid current of the inverter, while the associated harmonic spectra is shown in Fig. 18. It is clear that only the resonance closed to 1550 Hz is left in the simulated waveforms.

In contrast, Fig. 19 shows the simulated waveforms after enabling the active damper to suppress two resonances, and the corresponding harmonic spectra are depicted in Fig. 20. The effective damping of the double resonances by the active damper is observed. Fig. 21 gives the estimated frequencies by

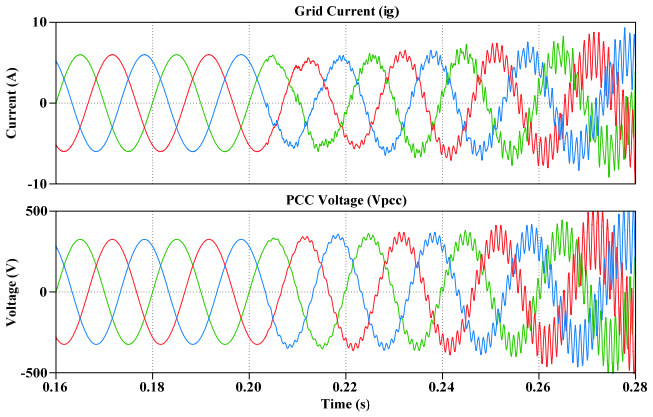

Fig. 15. Simulated inverter current and PCC voltage without enabling the active damper.

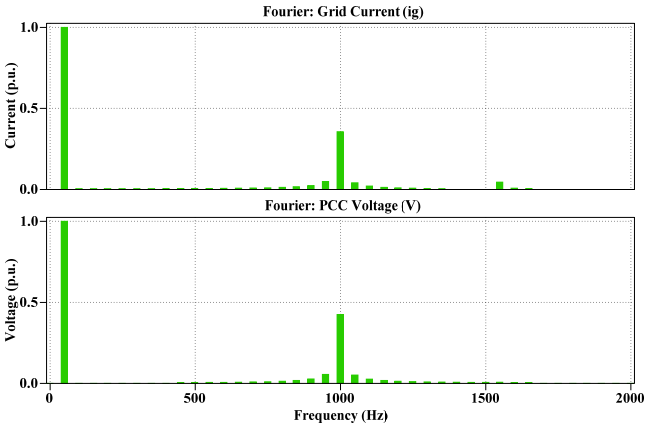

Fig. 16. Harmonic spectra for the simulated PCC voltage and grid current of the inverter in Fig. 15.

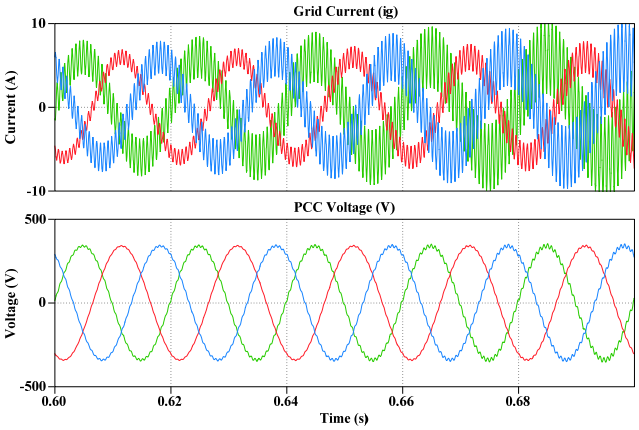

Fig. 17. Simulated PCC voltage and grid current of the inverter after enabling the active damper to only suppress the resonance around 1000 Hz.

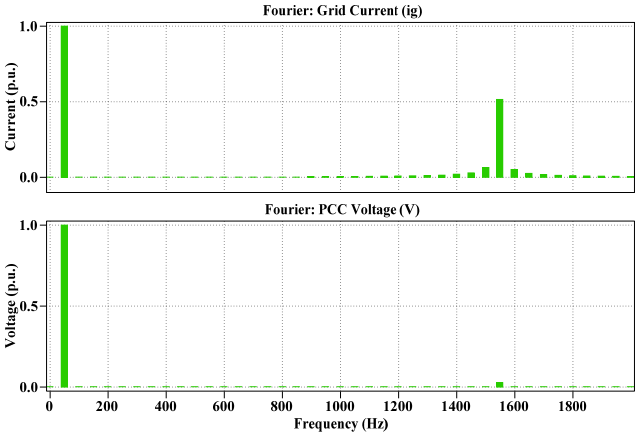

Fig. 18. Harmonic spectra for the simulated PCC voltage and grid current of the inverter in Fig. 17.

the cascaded ANF structure in this case. As the active damper is enabled after switching the inverter to the power cable at the time instant of 0.2 s, the frequency behavior of the cascaded ANF structure is shown after 0.2 s, which confirms again the performance of the cascaded ANF structure

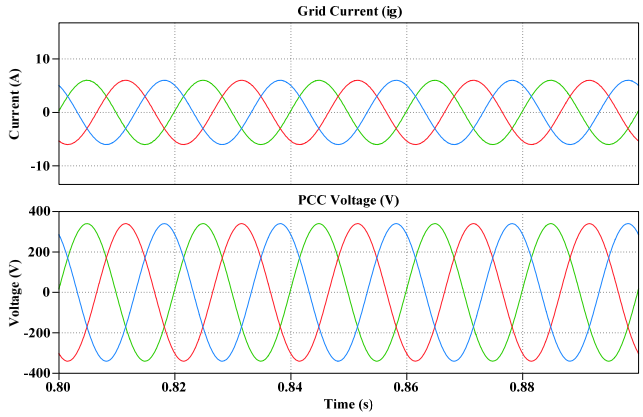

Fig. 19. Simulated PCC voltage and grid current of the inverter after enabling the active damper to suppress double resonances.

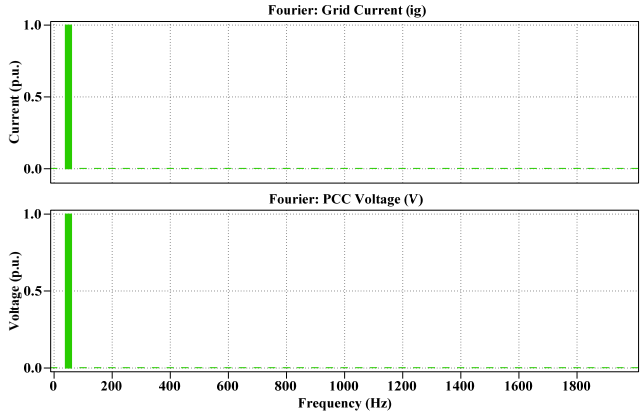

Fig. 20. Harmonic spectra for the simulated PCC voltage and grid current of the inverter in Fig. 19.

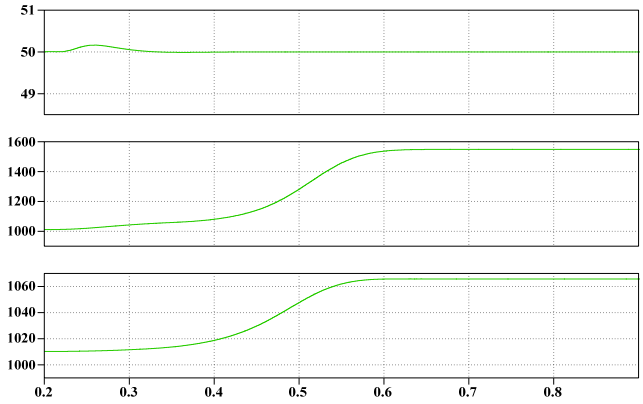

Fig. 21. Estimated frequencies by the cascaded ANF structure after enabling the active damper at 0.2 s.

VI. Conclusions

This paper has introduced an active damper which can suppress multiple resonances with unknown frequencies. The active damper is based on a high-bandwidth power converter, which selectively control the resonant voltages at the PCC of the grid-connected inverter. Further, a cascaded ANF-based FLL structure has been discussed, which enables the active damper to estimate the frequencies of resonances, and thus realizing the frequency adaptive control for the resonances in the system. The cascaded ANF structure is different from the parallel ANF structure with a common FLL, since the latter normally used to detect the harmonics that are correlated to the fundamental frequency signal and is thus sensitive to the interharmonics or resonances at the input signals. In contrast, the cascaded ANF structure provides a way to retrieve the sinusoids in noises. Both the frequency-domain analysis and time domain simulations have been presented to validate the performance of the active damper and the resonance frequency estimation method.

References

[1] F. Blaabjerg, Z. Chen, and S. B. Kjaer, "Power electronics as efficient interface in dispersed power generation systems," *IEEE Trans. Power Electron*., vol. 19, no. 5, pp. 1184-1194, Sept. 2004.

[2] X. Wang, J. M. Guerrero, F. Blaabjerg, and Z. Chen, "A review of power electronics based microgrids," *Journal of Power Electron.*, vol. 12, no. 1, pp. 181-192, Jan. 2012.

[3] Z. Shuai, D. Liu, J. Shen, C. Tu, Y. Cheng, and A. Luo, "Series and parallel resonance problem of wideband frequency harmonic and its elimination strategy," *IEEE Trans. Power Electron*., vol. 29, no. 4, pp. 1941-1952, Apr. 2014.

[4] M. Liserre, F. Blaabjerg, and S. Hansen, "Design and control of an *LCL*-filter-based three-phase active rectifier," *IEEE Trans. Ind. Appl*., vol. 41, no. 5, pp. 1281-1291, Sep./Oct. 2005.

[5] X. Wang, F. Blaabjerg, Z. Chen, and W. Wu, "Modeling and analysis of harmonic resonance in a power electronics based AC power system," in *Proc. IEEE ECCE* 2013, pp. 5529-5236.

[6] X. Wang, F. Blaabjerg, Z. Chen, and W. Wu, "Resoannce analysis in parallel voltage-controlled distributed generation inverters," in *Proc. IEEE APEC* 2013, pp. 2977-2983.

[7] F. Wang, J. L. Duarte, M. A. M. Hendrix, and P. F. Ribeiro, "Modeling and analysis of grid harmonic distortion impact of aggregated DG inverters," *IEEE Trans. Power Electron*., vol. 26, no. 3, pp. 786-797, Mar. 2011.

[8] S. Liang, Q. Hu, W. Lee, "A survey of harmonic emissions of a commecially operated wind farm," *IEEE Trans. Ind. Appl*., vol. 48, no. 3, pp. 1115-1123, May/Jun. 2012.

[9] J. Dannehl, M. Liserre, F. W. Fuchs, "Filter-based active damping of votlage source converters with *LCL* filter," *IEEE Trans. Ind. Electron*., vol. 58, no. 8, pp. 3623-3633, Aug. 2011.

[10] X. Wang, F. Blaabjerg, and Z. Chen, "Autonomous control of inverter-interfaced distributed generation units for harmonic current filtering and resonance damping in an islanded microgrid," *IEEE Trans. Ind. Appl*., Early Access Article, 2013.

[11] L. Harnefors, L. Zhang, and M. Bongiorno, "Frequency-domain passivity-based current controller design," *IET Power Electron.*, vol. 1, no. 4, pp. 455-465, Dec. 2008.

[12] T. Wang, Z. Ye, G. Sinha, and X. Yuan, "Output fitler design for a grid-interconnected three-phase inverter," in *Proc. IEEE APEC* 2003, vol. 2, pp. 779-784.

[13] M. Cespedes, L. Xing, and J. Sun, "Constant-power load system stabilization by passive damping," *IEEE Trans. Power Electron*., vol. 26, no. 7, pp. 1832-1836, Jul. 2011.

[14] R. N. Beres, X. Wang, F. Blaabjerg, M. Liserre, and C. L. Bak, "A review of passive filters for grid-connected voltage source converters," in *Proc. IEEE APEC* 2014, accepted.

[15] X. Wang, F. Blaabjerg, M. Liserre, Z. Chen, J. He, and Y. Li, "An active damper for stablizing power electronics based AC systems," *IEEE Trans. Power Electron*., Early Access Article, 2013.

[16] H. Akagi, H. Fujita, and K. Wada, "A shunt active filter based on voltage detection for harmonic termination of a radial power distribution line," *IEEE Trans. Ind. Appl.,* vol. 35, no. 3, pp. 638-645, May/Jun. 1999.

[17] S. Zhang, S. Jiang, X. Lu, B. Ge, and F. Z. Peng, "Resonance issues and damping techniques for grid-connected inverters with long transmission cable," *IEEE Trans. Power Electron*., vol. 29, no. 1, pp. 110-120, Jan. 2014.

[18] S. Parker, B. P. McGrath, and D. G. Holmes, "Region of active damping control for LCL filters," *IEEE Trans. Ind. Appl.*, Early Access Article, pp. 1-12, 2013.

[19] A. G. Yepes, F. Freijedo, O. Lopez, and J. Gandoy, "High-performance digital resonant controllers implemented with two integrators," *IEEE Trans. Power Electron*., vol. 26, no. 2, pp. 563-576, Feb. 2011.

[20] L. Asiminoaei, F. Blaabjerg, and S. Hansen, "Detection is key – harmonic detection methods for active power filter applications," *IEEE Ind. Appl. Mag.*, vol. 13, no. 4, pp. 22-33, Jul./Aug. 2007.

[21] E. Lavopa, P. Zanchetta, M. Sumner, and F. Cupertino, "Real-time estimation of fundamental frequency and harmonics for active shunt power filters in aircraft electrical systems," *IEEE Trans. Ind. Electron.,* vol. 56, no. 8, pp. 2875-2884, Aug. 2009.

[22] J. R. Glover Jr., "Adaptive noise canceling applied to sinusoidal interferences," *IEEE Trans. Acoust., Speech, Singal Process.,* vol. ASSP-25, no. 6, pp. 484-491, Dec. 1977.

[23] B. Widrow, J. R. Glover Jr., J. M. McCool, J. Kaunitz, C. S. Williams, R. H. Hearn, J. R. Zeidler, E. Dong Jr. and R. C. Googlin, "Adaptive noise canceling: principles and applications," in *Proc. IEEE*, vol. 73, no. 12, pp. 1692-1716, Dec. 1975.

[24] J. G. Mark, J. R. Steele, and C. C. Hansen, "Residual mode phase locked loop," U.S. Patent 4 495 475, Jan. 8, 1982.

[25] M. Bodson, "A discussion of Chaplin and Smith's Patent for the cancellation of repetitive vibrations," *IEEE Trans. Automat. Contr.,* vol. 44, no. 11, pp. 2221-2225, Nov. 1999.

[26] B. Wu and M. Bodson, "A magnitude/phase locked-loop approach to parameter estimation of periodic signals," *IEEE Trans. Automat. Contr.,* vol. 48, no. 4, pp. 612-618, Apr. 2003.

[27] X. Guo and M. Bodson, "Analysis and implementation of an adaptive algorithm for the rejection of multiple sinusoidal disturbances," *IEEE Trans. Control Syst. Technol.,* vol.17, no. 1, pp. 40-50, Jan. 2009.

[28] M. Karimi-Ghartemani and M. R. Iravani, "A nonlinear adaptive filter for on-line signal analysis in power systems: applications," *IEEE Trans. Power Del.,* vol. 17, no. 4, pp. 617-622, Apr. 2002.

[29] M. Karimi-Ghartemani and M. R. Iravani, "A method for synchronization of power electronic converters in polutted and variable-frequency environments," *IEEE Trans. Power Sys.,* vol. 19, no. 3, pp. 1263-1270, Aug. 2004.

[30] M. Karimi-Ghartemani, "A unifying approach to single-phase synchronous reference frame PLLs," *IEEE Trans. Power Electron*., vol. 28, no. 10, pp. 4550-4556, Oct. 2013.

[31] M. Karimi-Ghartemani, "A magnitude/phase-locked loop system based on estimation of frequency and in-phase/quadrature-phase applications," *IEEE Trans. Ind. Electron*., vol. 51, no. 2, pp. 511-517, Apr. 2004.

[32] M. Mojiri, M. Karimi-Ghartemani, and A. Bakhshai, "Estimation of power system frequency using adaptive notch filter," *IEEE Trans. Instrum. Meas.* vol. 56, no. 6, pp. 2470-2477, Dec. 2007.

[33] P. Rodriguez, A. Luna, R. S. Munoz-Aguilar, I. Qtadui, R. Teodorescu, and F. Blaabjerg, "A stationary reference frame grid synchronizaiton system for three-phase grid-connected power converters under adverse grid conditions," *IEEE Trans. Power Electron*., vol. 27, no. 1, pp. 99-112, Jan. 2012.

[34] P. Rodriguez, A. Luna, I. Candela, R. Mujal, R. Teodorescu, and F. Blaabjerg, "Multiresonant frequency-locked loop for grid synchronizaiton of power converters under distorted grid conditions," *IEEE Trans. Ind. Electron*., vol. 58, no. 1, pp. 127-138, Jan. 2011.

[35] J. Matas, M. Castilla, J. Miret, L. G. Vicuna, and R. Guzman, "An adaptive prefiltering method to improve the speed/accuracy tradeoff of voltage sequence detection methods under adverse grid conditions," *IEEE Trans. Ind. Electron*., vol. 61, no. 5, pp. 2139-2151, May 2014.